Dielectric function in the spectral range (0.5–8.5)eV of an $(Al_x Ga_{1-x})_2O_3$ thin film with continuous composition spread

R. Schmidt-Grund, C. Kranert, H. von Wenckstern, V. Zviagin, M. Lorenz, and M. Grundmann

Citation: Journal of Applied Physics **117**, 165307 (2015); doi: 10.1063/1.4919088
View online: https://doi.org/10.1063/1.4919088
View Table of Contents: http://aip.scitation.org/toc/jap/117/16
Published by the American Institute of Physics

JOURNAL OF APPLIED PHYSICS **117**, 165307 (2015)

Dielectric function in the spectral range (0.5–8.5)eV of an $(Al_xGa_{1-x})_2O_3$ thin film with continuous composition spread

R. Schmidt-Grund,[a] C. Kranert, H. von Wenckstern, V. Zviagin, M. Lorenz, and M. Grundmann
Fakultät für Physik und Geowissenschaften, Institut für Experimentelle Physik II, Universität Leipzig, Linnéstr. 5, D-04103 Leipzig, Germany

(Received 12 February 2015; accepted 2 April 2015; published online 28 April 2015)

We determined the dielectric function of the alloy system $(Al_xGa_{1-x})_2O_3$ by spectroscopic ellipsometry in the wide spectral range from 0.5 eV to 8.5 eV and for Al contents ranging from $x = 0.11$ to $x = 0.55$. For the composition range $x < 0.4$, we observe single phase material in the β-modification and for larger Al content also the occurrence of γ-$(Al,Ga)_2O_3$. We derived spectra of the refractive index and the absorption coefficient as well as energy parameters of electronic band-band transitions by model analysis of the dielectric function. The dependence of the dielectric functions lineshape and the energy parameters on x is highly continuous, reflecting theoretical expectations. The data presented here provide a basis for a deeper understanding of the electronic properties of this material system and may be useful for device engineering. © *2015 AIP Publishing LLC*. [http://dx.doi.org/10.1063/1.4919088]

I. INTRODUCTION

Due to its large band gap of approximately 5 eV, Ga_2O_3 is promising for applications such as high-power devices,[1] transparent electronics, and solar-blind ultraviolet (UV) photo-detectors.[2–6] For further increasing the band gap, e.g., for fabrication of heterostructures like quantum wells or detectors which are sensitive even deeper in the UV spectral range, the alloy system $(Al_xGa_{1-x})_2O_3$ is a promising candidate since the band gap energy can be increased to values larger 7.5 eV.[7,8]

Although theoretical understanding of wide band gap multicomponent oxides has moved more into focus of recent research (e.g., Refs. 9–11), detailed knowledge on basic optical properties such as the dielectric function spectra and properties of electronic band-band transitions of such materials is missing so far, even for the alloy system $(Al_xGa_{1-x})_2O_3$.

In this work, we present spectra of the dielectric function of $(Al_xGa_{1-x})_2O_3$ determined by spectroscopic ellipsometry for a large composition range $x = 0.11 - 0.55$ and for energies $(0.5 - 8.5)$ eV. We discuss their lineshape in comparison with theoretical predictions. By a lineshape model analysis of the dielectric functions (DF), we obtain spectra of the refractive index and absorption coefficient and derive energy parameters of band-band transitions.

As already discussed in Ref. 12, the electronic and optical properties in the near-infrared to vacuum-ultraviolet spectral range of different polymorphs of Ga_2O_3 have been thoroughly studied theoretically[13–16] but less comprehensively by experiment.[17–20] For Al_2O_3, more reports on theoretical and experimental work are available because its long term use as substrate material and insulating dielectric (for example Refs. 21–29). For the $(Al_xGa_{1-x})_2O_3$ alloy system, theoretical considerations are not available so far and only few experimental reports for the α-, β-, and γ-phase on growth and optical properties are available, but limited to band gap energies determined from transmission experiments.[7,8,30] A shift of the fundamental absorption edge from ≈5.25 eV for low Al content to values approaching more or less the band gap energy of Al_2O_3 was reported for the α-phase, showing a strong negative bowing in the composition dependence, especially for high Al contents.

The highest valence bands of β-Ga_2O_3 and α-Al_2O_3 consist mainly of O 2*p* orbitals.[13–15,21] For α-Al_2O_3, a split-off band formed by O 2*s* states is present and also Al 3*s* states contribute weakly and Al 3*p* as well as 3*d* states remarkably to the highest valence bands.[22–25] The lowest conduction bands of β-Ga_2O_3 are mainly due to Ga 4*s* orbitals, and those of α-Al_2O_3 are mainly due to Al 3*s* and at slightly higher energies Al 3*p* and 3*d* orbitals. Also, O 2*s* and 2*p* states contribute weakly.[22,23] For γ-Al_2O_3, the electronic structure is similar.[26,27]

The theoretically predicted spectra of the complex DF $\tilde{\varepsilon}$ for β-Ga_2O_3 (Refs. 14–16) yield the strongest absorption between 10 eV and 17 eV, and the onset of the absorption is clearly characterized by excitonic effects.[16] The lineshape of the DFs for both γ- and α-Al_2O_3 looks similar except for the energy blue shift.[23,24,27] Thus, we do not expect a significant change of the general shape of the DF spectra for the alloy system, although with increasing Al content the Al *p* and *d* orbitals contribute increasingly to the electronic structure and thus influence the optical band-band transition properties in the vicinity of the fundamental band gap.[11] Please note that we do not discuss the anisotropy of the optical properties because we have, due to the crystalline structure of our films, no access to the individual tensor elements of $\tilde{\varepsilon}$ (cf. also Sec. II B).

In the following, we introduce the experimental details in Sec. II, followed in Sec. III by the discussion of the dielectric function properties of the $(Al_xGa_{1-x})_2O_3$ alloy system in

[a]Schmidt-Grund@physik.uni-leipzig.de

the composition range $x = 0.11 - 0.55$ and for energies $(0.5 - 8.5)$ eV.

II. EXPERIMENTAL DETAILS

A. Samples

The $(Al_xGa_{1-x})_2O_3$ thin film sample with continuous composition spread (CCS) was grown by means of pulsed laser deposition (PLD) using a segmented PLD target (for further details on the PLD CCS technique see von Wenckstern *et al.*[31]) on a 2-in. (100)-oriented MgO substrate at a temperature of ≈650 °C without any post-treatment. The thickness of the film across the investigated composition range was found to be between 400 nm and 600 nm. More details on the growth conditions can be found in Ref. 32. As also detailed there, the composition as a function of the position on the wafer and the structural properties of the thin films have been investigated by means of energy dispersive X-Ray spectroscopy (EDX), X-Ray diffraction (XRD), and Raman spectroscopy. Figure 1 displays the Al concentration across the sample obtained from an EDX line scan. For low Al concentration, we found full incorporation of Al in the β-Ga_2O_3-lattice and thus single phase material with (100)-orientation. For Al concentration higher than ≈0.5, we found γ-phase $(Al_xGa_{1-x})_2O_3$.[32] XRD rocking curves, measured with a parabolic mirror and with fully open PIXcel^{3D} detector, yield high crystalline quality in the single phase composition range. The FWHM of the β-Ga_2O_3 (400) reflex is found to be ≈1° for $x < 0.4$. For larger x, the FWHM of this peak increases up to ≈2°, reflecting the phase transition accompanied possibly by phase separation.

B. Spectroscopic ellipsometry

The dielectric functions $\tilde{\varepsilon} = \varepsilon_1 + i\varepsilon_2$ of the thin film were determined by means of standard spectroscopic ellipsometry[33] in a wide spectral range from 0.5 to 8.5 eV at angles of incidence $\phi = 60°$ and 70° at room temperature. We used a commercial rotating analyser spectroscopic ellipsometer equipped with a automatic retarder in order to enhance the data accuracy, especially of the phase difference Δ between the p- and s-polarized eigenmodes.[42] The measurements were carried out along the Al gradient every 5 mm from edge to edge. Here, the light propagation direction was perpendicular to the Al gradient, and the spot size on the sample was approximately 3 mm in width and 5 mm long. Thus, for each measurement, a range of typically $\Delta x \approx 0.03$ with different Al concentrations, slightly depending on the position on the sample, is probed (Fig. 1). The sample's inhomogeneity within the area of the probe spot does not affect the accuracy of the ellipsometry data, as confirmed by spectra of the depolarization,[33] which yield within the whole composition and spectral range investigated very low values below 0.5% and only peak directly at the inset of absorption to values of 1.8% at very maximum, reflecting the composition gradient. Thus, for further analysis, no composition or thickness gradient for each position respective x-value investigated was assumed.

The experimental data are analysed using a transfer-matrix technique[33] with matrices representing each layer of the sample stack: half-infinite MgO substrate, the thin film of interest, and surface roughness. We took the substrate's DF from Ref. 34. The DFs of the materials were described by either analytic, lineshape function based parametric model-DFs (MDF, cf. Sec. III B 1) or numerically by Kramers-Kronig consistent mathematical approximation of the experimental data using B-spline functions.[35] The surface of the oxide thin films was assumed to show some roughness without any chemical modification; thus, a standard Bruggeman effective-medium approximation (EMA)[36] was applied, allowing for variable fractions in mixing of the dielectric functions of the thin film and void. Regression analysis using a Levenberg-Marquardt algorithm was applied to best match the model to the experimental data. Examples for the model approximation to the experimental data are shown in Fig. 2 by means of the complex pseudo dielectric function $\langle\tilde{\varepsilon}\rangle = \langle\varepsilon_1\rangle + i\langle\varepsilon_2\rangle$. The spectra of the real and imaginary part of the material

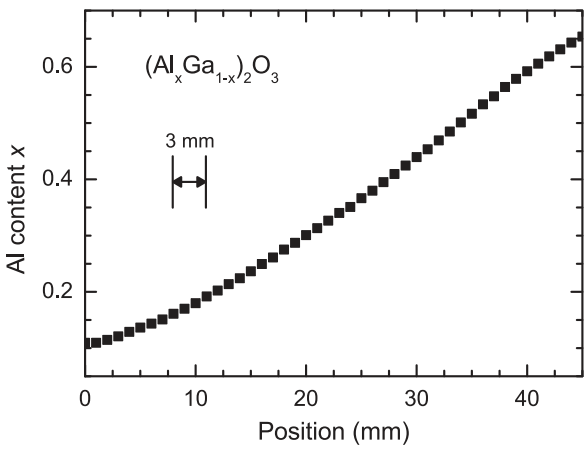

FIG. 1. Aluminium concentration x of the CCS sample obtained from an EDX line scan along the positions of the ellipsometry measurements. The relative uncertainty of the Ga concentration is in the order of 5%. The spatial resolution (≈3 mm) of the ellipsometry measurement is indicated.

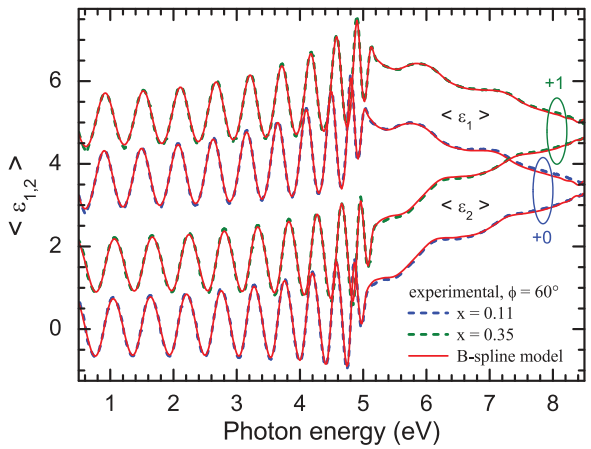

FIG. 2. Experimentally determined (dashed lines) and model-calculated (red solid lines) spectra of the pseudo dielectric functions $<\varepsilon_{1,2}>$ for selected Al concentrations x for an angle of incidence of $\phi = 60°$. The spectra are shifted vertically against each other for clarity as indicated in the figure. Please note the change in the period of the layer thickness interference pattern. The thickness of the film across the entire composition range investigated ranges between 400 nm and 600 nm.

dielectric function $\tilde{\varepsilon} = \varepsilon_1 + i\varepsilon_2$ obtained from the numeric B-spline modelling for all investigated compositions are shown in Fig. 3.

Please note that, similar to our investigations on $(In_xGa_{1-x})_2O_3$ thin films reported earlier,[12] we have determined the effective isotropic dielectric function[37] of this ternary alloy of optically biaxial and uniaxial binary materials. This was necessary because we have no access to the individual dielectric tensor components due to rotation domains and twinning of the crystallites and the occurrence of the different crystal structure phases in the thin films. Thus, some of the individual features may belong to different tensor elements and the determined energies, and the large broadening of the transitions observed may also be influenced by a superposition of the response from the individual tensor elements. But, the general trend in change of the lineshape and the composition evolution is considered reliable.

III. RESULTS AND DISCUSSION

A. Refractive index

As can be seen in Fig. 3, materials with low Al concentration are transparent in a wide spectral range, where the optical response is fully described by the real part of the DF which is related to the refractive index by $n = \sqrt{\varepsilon_1}$. For the Al concentration $x > 0.15$, a considerable absorption in the NIR spectral range sets in extending more and more to higher energies with the increase in x, as will be discussed in Sec. III B (inset in Fig. 3(b), also clearly visible in Fig. 3(a) by the resonance behaviour in ε_1 at low energies), restricting the transparency spectral range. Within that range, the energy dispersion of n can be described by the so-called Cauchy model[33] as follows (valid for $\alpha < 10\,\mathrm{cm}^{-1}$, α being the absorption coefficient, cf. Fig. 5):

$$n(\lambda) = A + \frac{B}{\lambda^2} + \frac{C}{\lambda^4}, \tag{1}$$

with λ being the vacuum wavelength of light in units of μm and A, B, C the so-called Cauchy parameters. Spectra of $n(E)$ are shown in Fig. 4(a), and the Cauchy parameters as a function of the composition are given in Fig. 4(b). A clear decrease of $n(E)$ with increasing x can be observed. For the smallest Al concentration, the Cauchy parameter $A \approx 1.9$, which is related to the high-frequency dielectric constant by $A \equiv n_\infty = \sqrt{\varepsilon_\infty}$, reflects well values reported for pure Ga_2O_3 or $(In_xGa_{1-x})_2O_3$ thin films with low In concentration of $n_\infty \approx 1.9$ (experiment[12,18]) and $n_\infty \approx 1.67\ldots1.69$ (theory[15]). For large x, it decreases towards the value for α-Al_2O_3 of $n_\infty \approx 1.75$.[28,29]

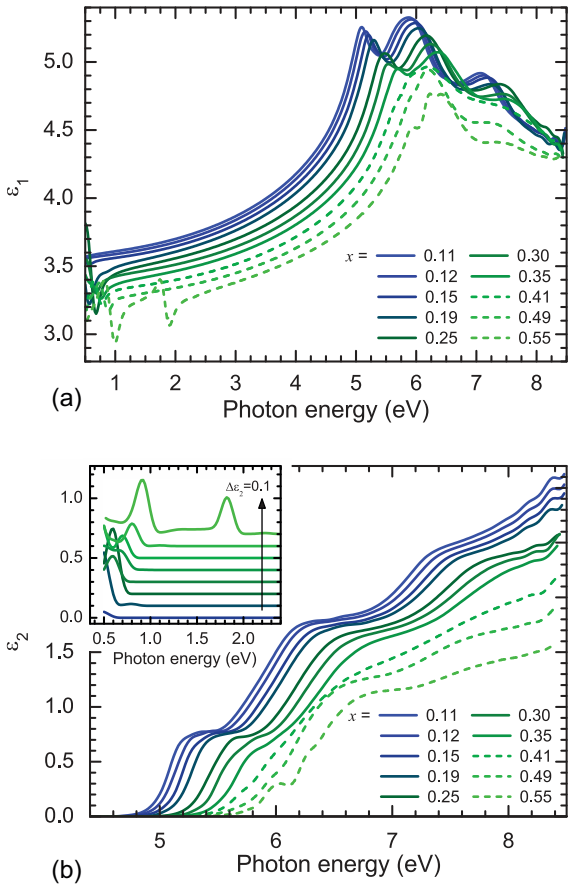

FIG. 3. Spectra of the (a) real (ε_1) and (b) imaginary part (ε_2) of the dielectric functions for all Al concentrations x investigated (B-spline model). Dashed lines indicate composition for which the γ-phase has been observed.[32] For ε_2, only the spectral range revealing non-vanishing values is shown. The inset displays the NIR spectral range showing absorption features arising with increasing Al content. Here, the spectra are shifted vertically against each other for clarity as indicated. A file containing the tabulated DF spectra for all compositions can be found in the supplementary material.[38]

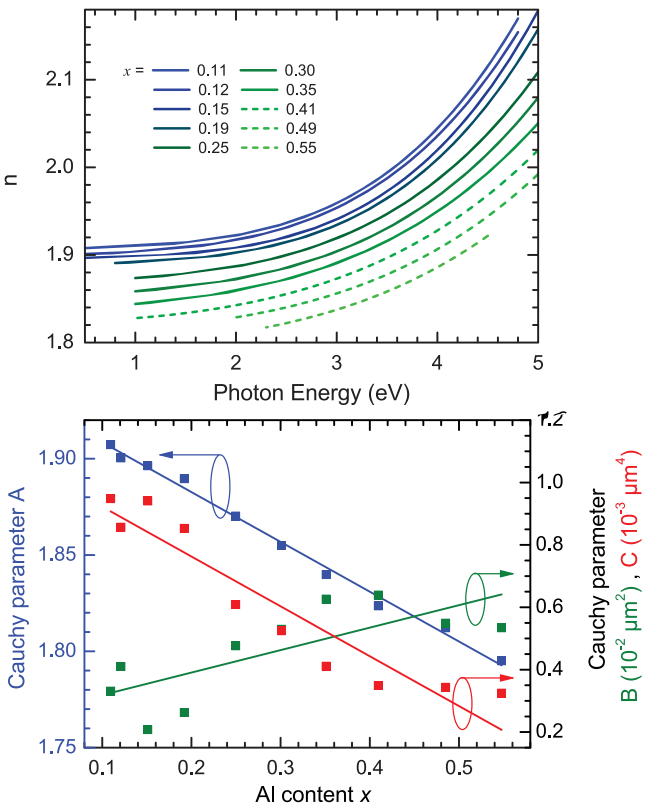

FIG. 4. (a) Spectra of the refractive index in the transparency spectral range for all x investigated. Dashed lines indicate composition for which the γ-phase has been observed.[32] (b) Parameters of the Cauchy model (Eq. (1)) as a function of x (symbols, lines are guides to the eye only). Please note that the scatter in the parameter values can largely be attributed to pronounced correlation between the Cauchy parameters in the regression analysis.

B. Dielectric function and absorption coefficient

The spectra of the DF and the absorption coefficient α are distinguished by the onset of strong absorption at $E \approx 4.8\ldots5.8$ eV for $x = 0.11\ldots0.55$ (Figs. 3 and 5(a), tabulated DF spectra are provided in the supplement.[38]). At higher energies, several features due to electronic transitions are observable. As mentioned above, materials with low Al concentration are transparent in the near-infrared to near-ultraviolet spectral range, while for Al concentration $x > 0.15$, a considerable absorption in the near-infrared spectral range sets in. This absorption yields characteristic features of discrete resonances visible in both ε_1 and ε_2 (Fig. 3(a) and the inset in Fig. 3(b)), which can be well-modelled by Lorentzian oscillators (cf. Fig. 7(b)). From these lineshapes, we suppose discrete plasmon resonances in phase separated Al nano-particles to be their origin.[39] This property is beyond the focus of the manuscript; thus, we will not discuss it in more detail. We assume that the electronic band-to-band absorption features as discussed below are not considerably affected except for a possible weak additional uncertainty in the Al content scale.

Remarkably, and different to the trend found for the $(In_xGa_{1-x})_2O_3$ alloy system,[12] the lineshape of the DF is almost the same for all compositions investigated. Some exception can be observed for $x > 0.4$, which we can relate to the occurrence of γ-phase material.[32] The general lineshape resembles that of pure β-Ga_2O_3;[12,14,15] thus, we conclude that the materials' electronic structure is dominantly β-Ga_2O_3-like for all Al concentrations investigated. A clear blue-shift of all absorption features can be observed as expected due to the much larger band gap of α- and γ-Al_2O_3 of $\approx$9 eV. As a general observation, the spectral broadening of the absorption features increases slightly with the increase in x as also the sub-band gap absorption tail increase slightly in spectral extend. From that, we conclude that the crystal quality in general is not strongly affected by Al incorporation, differently to In.[12] This may be related to the covalent radius of Al being similar to that of Ga, resulting in only a small variation of the lattice parameters with the composition, particularly as compared to $(In_xGa_{1-x})_2O_3$.[32,40] Much more pronounced than in the $(In_xGa_{1-x})_2O_3$ alloy system, the overall spectral weight of the electronic band-band transitions decreases considerably with the increase in Al incorporation in the spectral range investigated here. We do not expect such a strong change for electronic transitions at much higher energies, because ε_1 is very similar for all x at high energies around 8 eV. This behaviour of the spectral weight is also reflected in the strong change of the refractive index (Fig. 4).

We have analysed the absorption coefficient as determined from the numeric B-spline MDF regarding the type of the band gap. From its logarithmic representation (Fig. 5(b)), we determined a Tauc[41] absorption energy E_{g-log}, reflecting

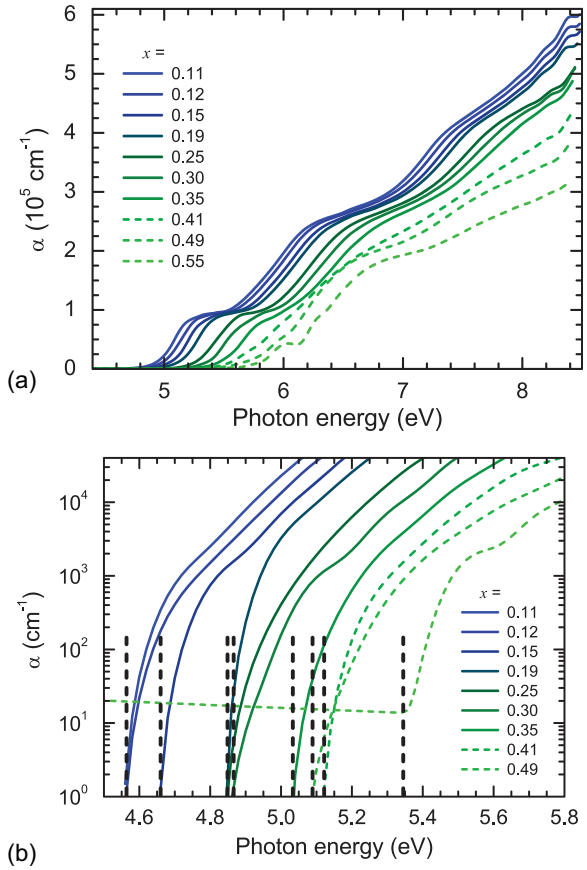

FIG. 5. Spectra of the absorption coefficient α in the UV spectral range calculated from the B-spline MDF in a (a) linear and (b) logarithmic scale. Dashed lines indicate composition for which the γ-phase has been observed.[32] Dashed black lines indicate the linear approximation and extrapolation of log α towards zero.

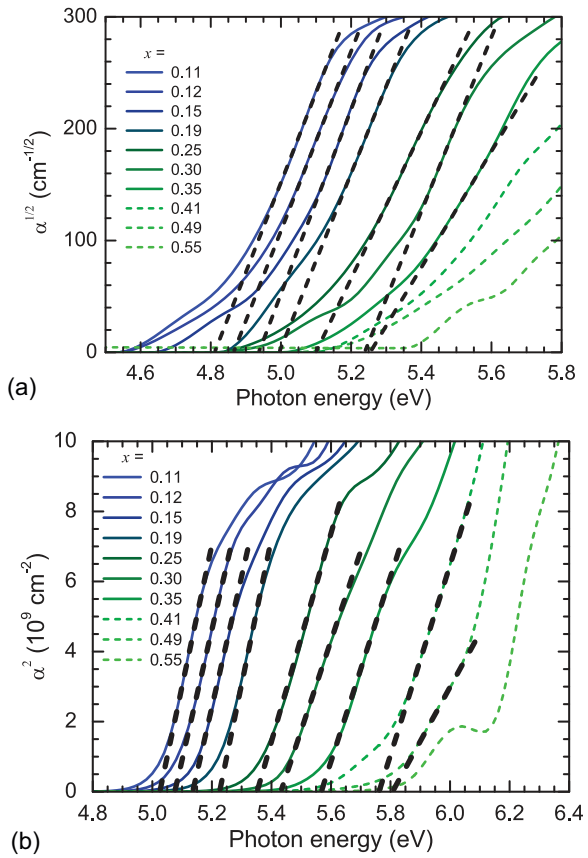

FIG. 6. Spectra of (a) $\sqrt{\alpha}$ and (b) α^2 calculated from the B-spline MDF. Dashed lines indicate composition for which the γ-phase has been observed.[32] Dashed black lines indicate linear extrapolation towards zero.

the fundamental absorption edge. At higher energies, a possible indirect absorption edge at E_{g-ind} can be estimated from linearly extrapolating $\sqrt{\alpha}$ vs. energy to zero (Fig. 6(a)), followed by a direct gap at E_{g-dir} determined from α^2 vs. energy (Fig. 6(b)). As both of the latter two approximations fit relatively well to the data, it cannot be decided whether the band gap type is direct or indirect, possibly both types occur spectrally close to each other. All these three energies yield an almost linear composition dependence shifting to higher energies with the increase in x as can be seen in Fig. 8(a) and which reproduces the trend found for the fundamental absorption edge energy in literature for the α-phase in this composition range.[7,8]

In the following, we will introduce the parametric MDF used to describe the lineshape of $\tilde{\varepsilon}$ and discuss the composition dependence of their parameters.

1. Model

Motivated by the lineshape of the numeric B-spline MDF and α spectra, we apply a similar parametrization of the DF as already used and discussed in detail for the $(In_xGa_{1-x})_2O_3$ alloy system.[12] We use an exponential onset of the absorption due to the disorder in the atomic site occupation in the ternary crystal and/or weak absorption caused by symmetry forbidden transitions or an indirect band gap. The appropriate MDF is the Tauc-Lorentz model,[41] which usually reads for ε_2 (ε_1 follows from the Kramers-Kronig transformation)

$$\varepsilon_{2,\mathrm{TcLo}}(E) = \begin{cases} 0 & 0 < E \le E_{g-\mathrm{TcLo}} \\ [T(E)\cdot L(E)] & E > E_{g-\mathrm{TcLo}}, \end{cases} \quad (2)$$

with the Tauc absorption,

$$T(E) = \frac{(E - E_{g-\mathrm{TcLo}})^2}{E^2}, \quad (3)$$

and the Lorentz oscillator

$$L(E) = \frac{AE_{n-\mathrm{TcLo}}\Gamma E}{\left[\left(E^2 - E_{n-\mathrm{TcLo}}^2\right)^2 + \Gamma^2 E^2\right]}, \quad (4)$$

E being the photon energy. The energy $E_{g-\mathrm{TcLo}}$ describes the usual band gap energy for parabolic bands and $E_{n-\mathrm{TcLo}}$ the resonance energy of the Lorentz oscillator. A and Γ denote the amplitude and the broadening of the Lorentz oscillator.

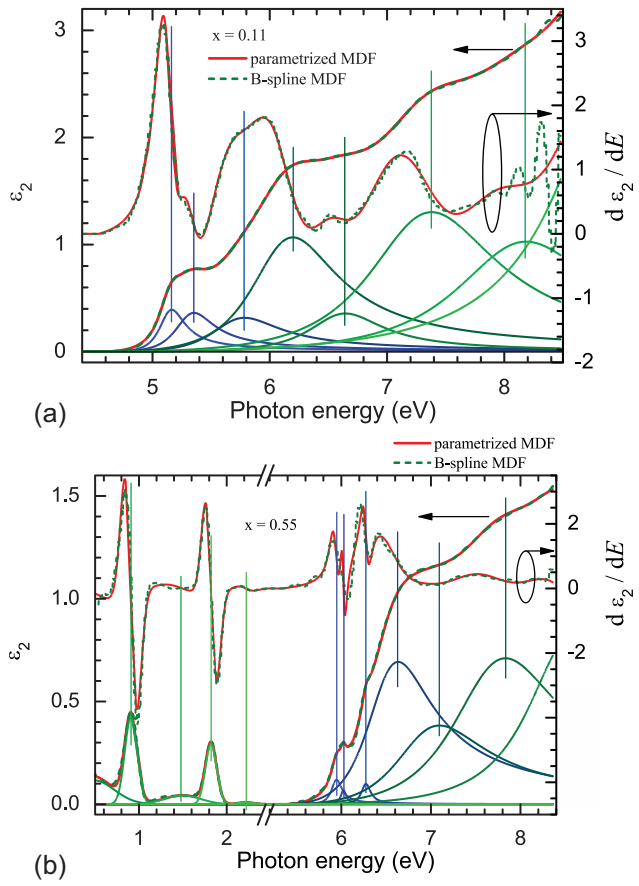

FIG. 7. Comparison of B-spline and parametrized model spectra of ε_2 and $d\varepsilon_2/dE$, exemplarily for (a) $x = 0.11$ and (b) $x = 0.55$. The individual contributions to the parametrized ε_2 model are included in blue… green coloured lines, which are the TcLo oscillators in the UV spectral range and Lorentzians and a Drude free charge carrier absorption term in the NIR spectral range. The vertical lines relate the peak energies of the model functions to features observed in the dielectric function. For $x = 0.11$, only the UV spectral range is shown because there is no low-energy absorption feature observable, while for $x = 0.55$ also the discrete absorption features in the NIR spectral range are included.

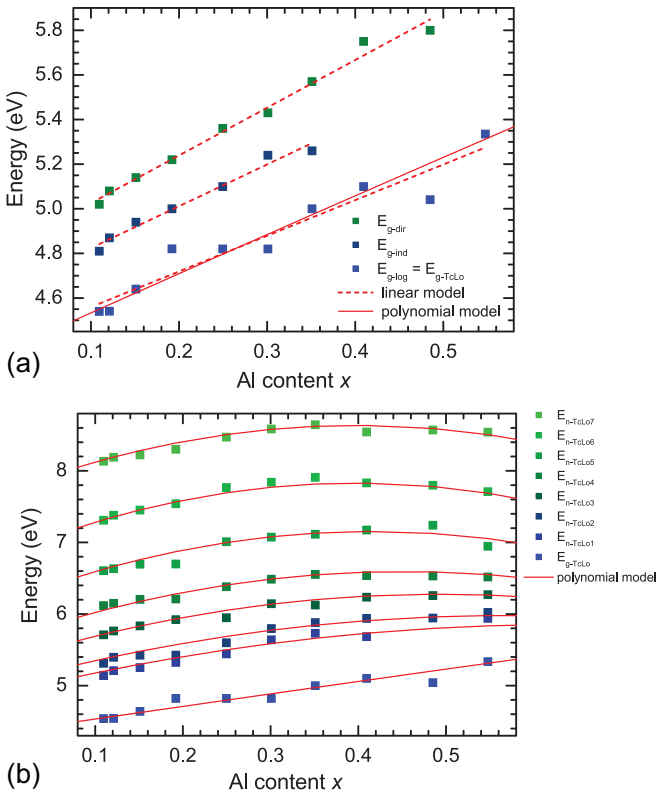

FIG. 8. (a) Energies of the absorption onset $E_{g-\log}$, of the indirect gap E_{g-ind}, and the direct gap E_{g-dir} obtained from the linear approximation and extrapolation towards zero of $\log\alpha$, $\sqrt{\alpha}$, and α^2, respectively, obtained from the B-spline MDF (cf. Figs. 5 and 6). (b) Energy parameters of all TcLo-MDF contributions TcLo1…TcLo7 (common $E_{g-\mathrm{TcLo}}$ and $E_{n-\mathrm{TcLo},i}$) obtained by the lineshape analysis of the MDF. In (a) and (b), the dashed red lines indicate a linear approximation of the energy dependence on x after Eq. (6), while the solid ones represent the polynomial approximation of the common model for all energies $E_{n-\mathrm{TcLo},i}$ after Eq. (7). The parameters of both models can be found in Table I.

TABLE I. Energy parameters of Eqs. (6) and (7) (cf. also Fig. 8). All energies are given in units of eV; the uncertainty is in the order of the last digit.

	E_{g-log}	E_{g-ind}	E_{g-dir}	E_{g-TcLo}	$E_{n-TcLo1}$	$E_{n-TcLo2}$	$E_{n-TcLo3}$	$E_{n-TcLo4}$	$E_{n-TcLo5}$	$E_{n-TcLo6}$	$E_{n-TcLo7}$
$E_{gi,0}$	4.40	4.637	4.811	…	…	…	…	…	…	…	…
$E_{gi,x}$	1.60	1.87	2.138	…	…	…	…	…	…	…	…
$E_{i,0}$	…	…	…	4.40	4.90	5.05	5.35	5.65	6.18	6.85	7.72

The electronic properties are apparently well-defined, which is reflected by the distinct features in the DF spectra for all investigated compositions. Thus, for the parametrized total MDF for each value of x, we could use a series of seven Tauc-Lorentz model functions (Eq. (2), "TcLo") joining all the same gap energy E_{g-TcLo} and a pole function (i.e., an undamped harmonic oscillator, "Pol") in order to account for contributions of electronic transitions to ε_1 at energies higher than the spectral range investigated here. The absorption features at low energies arising for $x \gtrsim 0.15$ are described by Lorentzian oscillators and a weak Drude term for free charge carrier absorption, considered in the MDF contribution $\tilde{\varepsilon}_{NIR}(E)$. The total parametric MDF reads

$$\tilde{\varepsilon}_{total}(E) = \sum_{i=1}^{7} \tilde{\varepsilon}_{TcLo,i}(E) + \tilde{\varepsilon}_{Pol}(E)(+\tilde{\varepsilon}_{NIR}(E)). \quad (5)$$

Examples for the approximation of the parametrized MDF to the numeric B-spline MDF are shown in Fig. 7 along with their individual contributions. The overall agreement is very good, especially considering the spectra of $d\varepsilon_2/dE$. Some deviations at higher energies may be caused in larger data uncertainty, but also some further weak band-band transition features could be present which are hard to the model caused by parameter correlation reasons.

2. Results

The energy parameters as a function of x obtained from the absorption coefficient and of the individual contributions to the parametrized MDF are shown in Fig. 8. An almost continuous blueshift within the entire composition range is observed as expected for incorporation of Al. The energies E_{g_i} obtained from the linear approximation and extrapolation towards zero of $\log \alpha$, $\sqrt{\alpha}$, and α^2, E_{g-log}, E_{g-ind}, and E_{g-dir}, respectively, based on the B-spline MDF depend almost linearly on x

$$E_{gi} = E_{gi,0} + E_{gi,x} \times x, \quad (6)$$

with $E_{gi,0}$ denoting the values for $x = 0$. The energies E_i of the parametric TcLo model approximation of the dielectric function E_{g-TcLo} and $E_{n-TcLo,j}$ ($j = 1 \ldots 7$) can be approximated regarding their composition dependence with a common polynomial equation

$$E_i = E_{i,0} + (-18.4[eV] + 6.78\,E_{i,0} - 0.49[eV^{-1}]\,E_{i,0}^2)x + (37.1[eV] - 12.4\,E_{i,0} + 0.89[eV^{-1}]\,E_{i,0}^2)x^2, \quad (7)$$

with $E_{i,0}$ denoting the values for $x = 0$. The parameters of Eqs. (6) and (7) can be found in Table I. It should be noted that we found E_{g-log} to be equal to E_{g-TcLo} within the data uncertainty. The increase of the transition energies, besides the effect of Al incorporation on the electronic structure, also resembles the behaviour of the lattice constants and the phonon modes.[32] Especially, the bowing observed for the thin film in the a-lattice constant, which we relate to internal strain, can be considered to be partially responsible for the bowing observed in the x-dependence of the transition energies.

As a general trend, the broadening parameter of the TcLo function increases with the increase in transition energy from ≈ 0.2 eV to ≈ 1.5 eV, but does almost not depend on x. The oscillator strength is found to be generally larger for oscillators at higher energies. Their composition dependence reflects basically the evolution of the spectral weight: For most of the oscillators, a strong, almost linear decrease with the increase in x is observed, while for those at around 6 eV and 6.5 eV, an increase is apparent.

It should be noted that the possibility to model the energy-x-dependence of the band-band transition features using a single formula gives strong hints on a continuous evolution of the electronic bandstructure via Al incorporation, even through the structural phase transition between the β- and γ-phase. Regarding the discussion in the introduction, we could expect exactly such a behaviour. The evolution of the DFs' lineshape with x further supports this continuity in the bandstructure properties. Further, we like to note that we cannot decide by our experimental data whether excitonic effects influence the lineshape of $\tilde{\varepsilon}$ respective α. Especially, the distinct onset of absorption could be also of excitonic origin as suggested by its resonance-like lineshape as visible in the derivative of ε_2 (Fig. 7).

IV. CONCLUSIONS

We have determined the DF of $(Al_xGa_{1-x})_2O_3$ thin films in a wide spectral range from near-infrared to vacuum-ultraviolet and for a large composition range $0.11 \leq x \leq 0.55$. We found an almost continuous evolution of the optical properties and thus the electronic structure with x, reflecting expectations from theory. In particular, the electronic structures of β- and γ-$(Al_xGa_{1-x})_2O_3$ appear to be similar for the investigated composition and spectral range. For $x > 0.15$, we found an arising absorption in the near-infrared which we relate to plasmonic effects in some segregated Al nanoparticles.

ACKNOWLEDGMENTS

We acknowledge Jörg Lenzner for EDX measurements of the thin films, Gabriele Ramm for the preparation of the PLD targets, Holger Hochmuth for thin film growth, as well as Helena Franke and Chris Sturm for comments on the manuscript and valuable discussions. This work was supported within the framework of EFRE (SAB 100132251).

C.K. was funded by the European Union and the Free State of Saxony.

[1]M. Higashiwaki, K. Sasaki, A. Kuramata, T. Masui, and S. Yamakoshi, Appl. Phys. Lett. **100**, 013504 (2012).
[2]T. Oshima, T. Okuno, N. Arai, N. Suzuki, S. Ohira, and S. Fujita, Appl. Phys. Express **1**, 011202 (2008).
[3]T. Oshima, T. Okuno, and S. Fujita, Jpn. J. Appl. Phys., Part 1 **46**, 7217 (2007).
[4]Y. Kokubun, K. Miura, F. Endo, and S. Nakagomi, Appl. Phys. Lett. **90**, 031912 (2007).
[5]H. von Wenckstern, Z. Zhang, J. Lenzner, F. Schmidt, and M. Grundmann, Proc. Mater. Res. Soc. **1633**, 123–129 (2014).
[6]H. von Wenckstern, D. Splith, M. Purfrst, Z. Zhang, C. Kranert, S. Müller, M. Lorenz, and M. Grundmann, Semicond. Sci. Technol. **30**, 024005 (2015).
[7]F. Zhang, K. Saito, T. Tanaka, M. Nishio, M. Arita, and Q. Guo, Appl. Phys. Lett. **105**, 162107 (2014).
[8]H. Ito, K. Kaneko, and S. Fujita, Jpn. J. Appl. Phys., Part 1 **51**, 100207 (2012).
[9]A. Walsh, J. L. F. Da Silva, and S.-H. Wei, J. Phys.: Condens. Matter **23**, 334210 (2011).
[10]A. Murat and J. E. Medvedeva, Phys. Rev. B **85**, 155101 (2012).
[11]K. Umemotot and R. M. Wentzcovitch, Phys. Chem. Minerals **38**, 387 (2011).
[12]R. Schmidt-Grund, C. Kranert, T. Böntgen, H. von Wenckstern, H. Krauß, and M. Grundmann, J. Appl. Phys. **116**, 053510 (2014).
[13]H. He, M. A. Blanco, and R. Pandey, Appl. Phys. Lett. **88**, 261904 (2006).
[14]K. Yamaguchi, Solid State Commun. **131**, 739 (2004).
[15]H. He, R. Orlando, M. A. Blanco, and R. Pandey, Phys. Rev. B **74**, 195123 (2006).
[16]J. B. Varley and A. Schleife, Semicond. Sci. Technol. **30**, 024010 (2015).
[17]N. Ueda, H. Hosono, R. Waseda, and H. Kawazoe, Appl. Phys. Lett. **71**, 933 (1997).
[18]M. Rebien, W. Henrion, M. Hong, J. P. Mannaerts, and M. Fleischer, Appl. Phys. Lett. **81**, 250 (2002).
[19]E. G. Víllora, M. Yamaga, T. Inoue, S. Yabasti, Y. Masui, T. Sugawara, and T. Fukuda, Jpn. J. Appl. Phys., Part 2 **41**, L622 (2002).
[20]M. Yamaga, T. Ishikawa, M. Yoshida, T. Hasegawa, E. G. Villora, and K. Shimamura, Phys. Status Solidi C **8**, 2621 (2011).
[21]I. P. Batra, J. Phys. C **15**, 5399 (1982).
[22]L. Salasco, R. Dovesi, R. Orlando, M. Causa, and V. R. Saunders, Mol. Phys. **72**, 267 (1991).
[23]W. Y. Ching and Y.-N. Xu, J. Am. Ceram. Soc. **77**, 404 (1994).
[24]B. Holm, R. Ahuja, Y. Yourdshahyan, B. Johansson, and B. I. Lundqvist, Phys. Rev. B **59**, 12777 (1999).
[25]T. V. Perevalov, A. V. Shaposhnikov, V. A. Gritsenko, H. Wong, J. H. Han, and C. W. Kim, JETP Lett. **85**, 165 (2007).
[26]G. Gutiérrez, Ad. Taga, and B. Johansson, Phys. Rev. B **65**, 012101 (2001).
[27]R. Ahuja, J. M. Osorio-Guillen, J. Souza de Almeida, B. Holm, W. Y. Ching, and B. Johansson, J. Phys.: Condens. Matter **16**, 2891 (2004).
[28]A. K. Harman, S. Ninomiyda, and S. Adachi, J. Appl. Phys. **76**, 8032 (1994).
[29]H. Yao and C. H. Yan, J. Appl. Phys. **85**, 6717 (1999).
[30]T. Oshima, T. Okuno, N. Arai, Y. Kobayashi, and S. Fujita, Jpn. J. Appl. Phys., Part 1 **48**, 070202 (2009).
[31]H. von Wenckstern, Z. Zhang, F. Schmidt, J. Lenzner, H. Hochmuth, and M. Grundmann, CrystEngComm **15**, 10020 (2013).
[32]C. Kranert, M. Jenderka, J. Lenzner, M. Lorenz, H. von Wenckstern, R. Schmidt-Grund, and M. Grundmann, J. Appl. Phys. **117**, 125703 (2015).
[33]H. Fujiwara, *Spectroscopic Ellipsometry: Principles and Applications* (John Wiley and Sons, New York, 2007).
[34]R. A. Synowicki and T. E. Tiwald, Thin Solid Films **455–456**, 248 (2004).
[35]B. Johs and J. S. Hale, Phys. Status Solidi A **205**, 715 (2008).
[36]J. Jellison, L. A. Boatner, D. H. Lowndes, R. A. McKee, and M. Godbole, Appl. Opt. **33**, 6053 (1994).
[37]S. Shokhovets, L. Spie, and G. Gobsch, J. Appl. Phys. **107**, 023509 (2010).
[38]See supplementary material at http://dx.doi.org/10.1063/1.4919088 for a file containing tabulated dielectric functions of the $(AlxGa_{1-x})_2O_3$ films discussed here.
[39]T. W. H. Oates, H. Wormeester, and H. Arwin, Prog. Surf. Sci. **86**, 328 (2011).
[40]C. Kranert, J. Lenzner, M. Jenderka, M. Lorenz, H. von Wenckstern, R. Schmidt-Grund, and M. Grundmann, J. Appl. Phys. **116**, 013505 (2014).
[41]G. E. Jellison and F. A. Modine, Appl. Phys. Lett. **69**, 2137 (1996); **69**, 371 (1996).
[42]p and s refers to the linear light polarization parallel and perpendicular to the plane of incidence which is spanned by the beam's propagation direction and the sample's surface normal. Further, the ellipsometric angle ψ varies between $\approx 2^\circ$ and $\approx 20^\circ$ as the minimum and maximum values of the thickness interference fringes for $\phi = 60^\circ$ and 70°, respectively, while Δ covers values within a range of 2π. Thus, a sufficient data accuracy is ensured.